Sensors and Actuators A 178 (2012) 40–48

Contents lists available at SciVerse ScienceDirect

Sensors and Actuators A: Physical

journal homepage: www.elsevier.com/locate/sna

Design, fabrication and characterization of high temperature piezoelectric vibration sensor using YCOB crystals

Kyungrim Kim [a], Shujun Zhang [b], Giovanni Salazar [a], Xiaoning Jiang [a,*]

[a] Department of Mechanical and Aerospace Engineering, North Carolina State University, Raleigh, NC 27695, USA
[b] Materials Research Institute, Pennsylvania State University, University Park, PA 16802, USA

ARTICLE INFO

Article history:
Received 21 June 2011
Received in revised form 31 January 2012
Accepted 5 February 2012
Available online 14 February 2012

Keywords:
Piezoelectric sensor
High temperature
Shear-mode accelerometer
YCOB

ABSTRACT

A shear-mode piezoelectric accelerometer using $YCa_4O(BO_3)_3$ single crystals (YCOB) was designed, fabricated and successfully tested for high temperature vibration sensing applications. Dynamic modeling of the accelerometer was presented first, followed by YCOB single crystal sample preparation, sensor assembly and experimental setup establishment. The prototyped accelerometer was tested at temperatures ranging from room temperature to 1000 °C and at frequencies ranging from 50 Hz to 350 Hz. The sensitivity of the prototype was found to be 5.9 ± 0.06 pC/g throughout the tested frequency, temperature and acceleration ranges. In addition, YCOB piezoelectric accelerometers retained the same sensitivity at 1000 °C for a dwell time of 9 h, exhibiting a high stability and reliability.

1. Introduction

In aerospace propulsion systems, high temperature (HT) sensors are required for intelligent propulsion system design and operation, and for enhancement of system maintenance and safety. Automotive combustion parts including injectors and valves for operations with repeated high temperature cycles require monitoring of ignition timing and the shape of the pulse for high combustion efficiency [1–5]. For reliable monitoring, sensors need to be located as close as possible to the high temperature source (e.g. engine) [6–9]. HT sensors for these applications are usually required to work properly at high temperatures greater than 1000 °C. To date, many types of sensors such as thermocouples, resistance temperature detectors (RTD), silicon carbide (SiC) sensors, and fiber optic sensors have been developed for high temperature applications [10,11]. Thermocouples have been most widely used as thermometers in laboratories and factories since temperatures can be directly measured up to 1750 °C. Silicon carbide (SiC) is one of the most promising semiconductors for implementing 400–600 °C integrated electronics due to its prominent electrical and mechanical properties, and chemical stability. Furthermore, competing electronics technologies such as silicon and silicon-on-insulator are physically incapable of functioning at high temperatures, or are significantly less-developed (GaN, diamond, etc.). Fiber optic sensors are also widely used in hostile environments due to their immunity to electromagnetic interference and intrinsic safety. However, challenges remain in fiber optic sensors such as fabrication complexity and expensive signal processing system [12,13]. While the above HT sensors can be applied in a broad range of HT applications, HT accelerometers for vibration sensing remains to be a challenge. The traditional types of accelerometers are piezoresistive-type and capacitive-type accelerometers which are based on silicon devices [1]. Piezoresistive accelerometers are less susceptible to electromagnetic interference (EMI) compared to capacitive accelerometers but they are not suitable for high temperature applications due to the temperature dependence of the resistivity [14,15]. Capacitive accelerometers have the advantage of low thermal drift, high resolution and good noise performance. This type of sensor could suffer from the influence of parasitic capacitance which can have similar value as capacitance of the sensors [16–18]. Fiber optic HT accelerometers are tolerant to electromagnetic interference and can offer reduced weight, and high operating temperature (<2000 °C) [19]. Up to date, HT accelerometers with simple structures, high sensitivity, high stability, long life time and higher operation temperature range have been actively investigated [1,2,11].

High temperature piezoelectric accelerometers are of particular interest because they have simple structures, fast response time, and easy integration with other parts where the high temperature piezoelectric materials are the mainstay [10]. Various types of piezoelectric materials for high temperature applications have been developed including quartz (SiO_2), lithium niobate

* Corresponding author at: Department of Mechanical and Aerospace Engineering911 Oval Drive, Engineering Building III, North Carolina State University, Raleigh, NC 27695, USA.
E-mail address: xjiang5@ncsu.edu (X. Jiang).

0924-4247/$ – see front matter © 2012 Elsevier B.V. All rights reserved.
doi:10.1016/j.sna.2012.02.003

($LiNbO_3$, LN), gallium orthophosphate ($GaPO_4$), langasite (LGS) and aluminum nitride (AIN). Quartz is one of the most widely used piezoelectric materials in electronic devices since it has excellent electrical resistivity (higher than 10^{17} Ω cm at room temperature), ultralow mechanical loss (high mechanical quality factor), narrow bandwidth, high stability when exposed to high temperatures. However, the use of quartz at high temperatures is limited by high losses above about 450 °C and α to β phase transition temperature at 573 °C [20,21]. $LiNbO_3$ possesses interesting properties at room temperature including high electromechanical coefficients. At high temperature, however, this material suffers from chemical decomposition (starts at 300 °C), increased attenuation and intergrowth transition. Furthermore, the lifetime of $LiNbO_3$ is limited to 10 days at 400 °C and 0.1 days at 450 °C due to its decomposition [22–24]. $GaPO_4$ has been extensively studied for various applications since it has high mechanical quality factor (about 20,000 at room temperature) as well as high electromechanical coupling and greater piezoelectric sensitivity below the phase transition temperature at 970 °C. However, the mechanical quality factor decreases significantly at temperatures above 700 °C as the structural disorder increases [25,26]. Langasite also has been extensively investigated because of its lack of phase transition prior to its melting point (1470 °C) as well as the availability of high quality crystals. However, the sensing capabilities of resonant devices made from langasite can be limited because the increased conductivity leads to decreased quality factor at elevated temperatures due to oxygen ion transport and diffusion in the lattice [26–29]. Aluminum nitride (AIN) has gained much attention for high temperature applications. AIN is an intrinsically poled, non-ferroelectric material which has no known Curie point. It can maintain its piezoelectric properties up to 1150 °C. This material is also a strong candidate for high frequency ultrasonic transducers since the deposition of thin films can be easily done, but it is tough to get good quality and large size bulk material [30–32]. On the other hand, recently discovered piezoelectric single crystal yttrium calcium oxyborate $YCa_4O(BO_3)_3$ (YCOB) is known for its stable piezoelectric properties at high temperature. Due to the absence of phase transitions up to its melting point (~1500 °C) and its phenomenon high resistivity, YCOB has been reported as a promising high temperature sensing crystal [3–5].

A high temperature piezoelectric accelerometer using YCOB monolithic compression-mode was fabricated and tested recently, demonstrating stable performances at high temperature up to 1000 °C [10]. Generally, for high temperature sensors, thin film electrodes (~100 nm thickness) capable of withstanding high temperature operation are essential [33,34]. Various thin film electrodes, including Pt/Zr, Ir/TiAlN, IrO_2/Ti, Pt/Ir and Pt/Rh, have been developed for high temperature applications. Nonetheless, their operating temperature is limited by the degradation at temperatures above 700 °C [35–40]. Therefore, high temperature sensors without thin film electrodes are attractive for reliable high temperature applications. Initial study finds that the absence of thin film electrodes in the sensor structure provides more stable performance of the accelerometer at high temperatures because there is no degradation of thin film electrode at elevated temperatures [41–43]. But the poor electric contact for piezoelectric sensors without thin film electrodes could lead to decreased sensitivity.

A shear mode YCOB high temperature vibration sensor without thin film electrodes was demonstrated recently in authors' lab and initial test results were reported in [44]. In this paper, details on design, fabrication and testing of a shear-mode piezoelectric accelerometer using YCOB crystals are presented. Unlike previous work, a lock-in amplifier was used to avoid the noise from power sources (60 Hz) which could affect the sensitivity of the sensor. Furthermore, dynamic model of shear-mode YCOB vibration sensor was, for the first time, established and compared to experimental results. YCOB sample preparation, sensor assembly and experimental setup were described in details. In addition, the tested frequency range was changed to a lower frequency to avoid resonance frequency and longer dwelling time test was performed successfully. The prototyped accelerometer was tested at the temperature ranging from room temperature to 1000 °C and at frequency ranging from 50 Hz to 350 Hz. The sensor stability and reliability were also measured for dwelling test at 1000 °C.

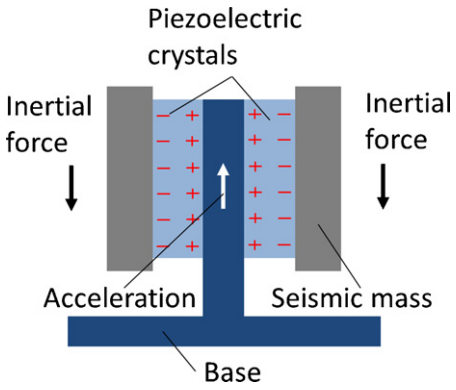

Fig. 1. A schematic sketch of a shear-mode piezoelectric sensor.

2. Sensor design and experimental setup

2.1. Shear-mode sensor modeling

Fig. 1 shows the schematic sketch of a shear-mode piezoelectric sensor. When the substrate is vibrating, an inertial force is generated and applied to the piezoelectric crystals and hence charge is generated. Charge output from piezoelectric crystals is proportional to the acceleration of the seismic mass. In a typical shear-mode accelerometer design, the sensing crystals are clamped or bonded between a center post and seismic masses. Under acceleration, a shear stress from the seismic mass is applied to the sensing crystal, generating a charge signal. By separating the sensing crystals from the base, reduced thermal transient and base bending effects can be obtained in comparison with other types of accelerometers.

For the dynamic response model, the accelerometer system can be divided by a mechanical and electrical system [45]. The differential equation of a vibrating system can be derived from the free body diagram of the accelerometer, as shown in Fig. 2:

$$m\ddot{x}_i = m\ddot{x}_0 + c\dot{x}_0 + kx_0 \quad (1)$$

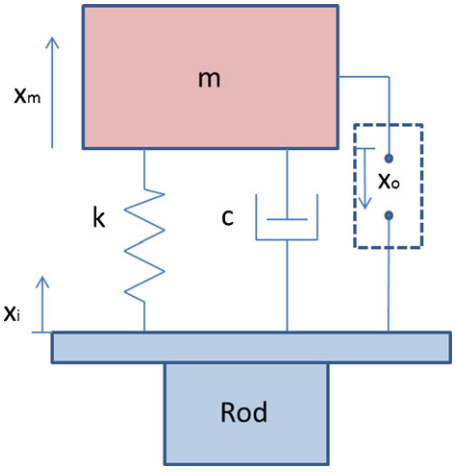

Fig. 2. Free body diagram of shear-mode accelerometer.

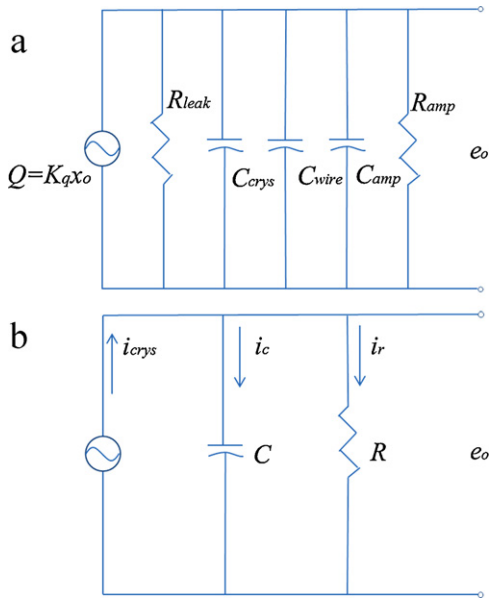

Fig. 3. (a) Electric circuit and (b) equivalent circuit of the shear-mode accelerometer.

where m, c, k, x_i, x_o are the seismic mass, the damping coefficient, the spring constant, the shaker displacement, the relative displacement between the seismic masses and the shaker. Assuming the initial condition is,

$$x_0(0) = \dot{x}_0(0) = 0 \tag{2}$$

Using the Laplace transformation, Eq. (1) can be expressed by the mechanical transfer function, H_m, which shows the relation between the input acceleration and the relative displacement:

$$H_m(s) = \frac{x_0(s)}{\ddot{x}_0(s)} = \frac{m}{k}\frac{\omega_n^2}{s^2 + 2\xi\omega_n s + \omega_n^2} \tag{3}$$

where ω_n is the resonant frequency of the sensor device and ξ is the damping ratio. The resonant frequency can be estimated by the following equation.

$$\omega_n = \sqrt{\frac{k}{m}} \tag{4}$$

$$f_n = \frac{1}{2\pi}\sqrt{\frac{k}{m}} \tag{5}$$

In electrical system, the relationship between the output charge and relative displacement is:

$$Q = k_q x_0 \tag{6}$$

$$k_q = \frac{AG}{l} d_{26} \tag{7}$$

where k_q, A, G, and l are the charge output of unit displacement, the area of the crystal, the shear modulus and the length of the crystal, respectively. From the electric model of the accelerometer (Fig. 3), the electric system governing equation can be derived as follow:

$$R = \frac{R_{amp}R_{leak}}{R_{amp} + R_{leak}} \cong R_{amp} \tag{8}$$

$$C = C_{Crys} + C_{wire} + C_{amp} \tag{9}$$

$$\dot{v}_0 = \frac{k_q}{C}\dot{x}_0 - \frac{v_0}{\tau} \tag{10}$$

where R_{amp} and R_{leak}, are resistance of the amplifier and crystal, C_{crys}, C_{wire} and C_{amp} are capacitance of the crystals, wires and the amplifier, v_o is output voltage from the sensor and τ is RC time constant, respectively. By applying the Laplace transformation to Eq. (10), the electrical transfer function (H_e) which shows the relation between the relative displacement and output voltage is:

$$H_e(s) = \frac{v_o(s)}{x_o(s)} = \frac{k_q}{C}\frac{\tau s}{\tau s + 1} \tag{11}$$

The dynamic response model of the accelerometer can be completed by combining the mechanical and electrical function as following:

$$\frac{v_o(s)}{\ddot{x}_i(s)} = S_T \frac{\tau s}{\tau s + 1}\frac{\omega_n^2}{s^2 + 2\xi\omega_n s + \omega_n^2} \tag{12}$$

The magnitude ratio can be found from Eq. (12) by substituting the frequency operator $j\omega$ for s. At the flat frequency response range, $\omega \gg 1/\tau$ and $\omega_n \gg \omega$, the voltage sensitivity, S_T, and the charge sensitivity, S_Q, at low frequencies can be approximated as follows:

$$S_T = \frac{k_q}{C}\frac{m}{k} \tag{13}$$

$$S_Q = S_T \times C = k_q \frac{m}{k} \tag{14}$$

2.2. YCOB crystals preparation

The raw materials Y_2O_3 (PIDC, 4 N-99.99% purity), $CaCO_3$ (Alfa Aesar, 4 N) and H_3BO_3 (Alfa Aesar, 4 N) were weighed according to the nominal composition and mixed. The YCOB compound was synthesized by calcining the mixed powder at 1000 °C for 10 h, and then sintered at 1250 °C to further shrink the volume for crucible filling. The sintered materials were loaded into an iridium crucible and melted at 1530 °C. The crystals were grown by the Czochralski pulling technique using a crystal pulling system. The atmosphere was nitrogen with 4% volume oxygen for all melting and growth stages. The crystal-pulling rate was on the order of 1 mm/h with a rotation of 15–30 rpm. The as-grown crystal boule(s) were slowly cooled down to room temperature over a 24-h period, to avoid the cracking [46]. YCOB is a monoclinic biaxial crystal belonging to the space group C_m. The physical axes X, Y, Z were determined according to the IEEE Piezoelectric Standard [47], where the Y axis is parallel to the b axis, Z to the c axis, and the X axis is perpendicular to both the Y and the Z axes to form a right-hand orthogonal system. In this study, thickness shear mode was used in the accelerometer design. Based on earlier investigations, (YXt) −30° cut samples exhibited the highest thickness shear piezoelectric and electromechanical properties [48], thus, (YXt) −30° cut samples with dimensions of 20 mm × 10 mm × 1 mm were prepared and polished using SiC powder. Then platinum thin film electrodes were deposited by vacuum sputtering for electrical measurements. The capacitance of the sample was measured at 100 kHz frequency using HP4284A multi-frequency LCR meter, while the resonance and anti-resonance frequencies of the thickness shear vibration were recorded by HP4294A impedance phase-gain analyzer, from which, the coupling k_{26}, elastic compliance s_{66} and piezoelectric constants d_{26} and g_{26} were calculated according to the following formulae [3–5]:

$$k_{26}^2 = \frac{\pi}{2}\frac{f_r}{f_a}\cot\left(\frac{\pi}{2}\frac{f_r}{f_a}\right) \tag{15}$$

$$S_{66}^E = \frac{1}{4\rho t^2 f_a^2(1 - k_{26}^2)} \tag{16}$$

$$d_{26}^2 = k_{26}^2 \times s_{66}^E \times \left(\frac{\varepsilon_{22}^T}{\varepsilon_0}\right) \tag{17}$$

$$g_{26} = \frac{d_{26}}{\varepsilon_{22}^T} \tag{18}$$

Table 1
Properties of YCOB crystals.

Crystal cut	ε_r	k_{26}	d_{26} (pC/N)	g_{26} (Vm/N)	S^E_{66} (m^2/N)	Q_{26}	ρ (Ω cm)
YXt 0°	12.3	0.19	8.0	0.07	0.17×10^{-10}	9000	2×10^7 (@ 950 °C)
YXt −30°	12.3	0.22	10	0.09	0.18×10^{-10}	16,000	

where f_r, f_a, ε^T_{22}, and ε_0 are the resonance frequency, anti-resonance frequency, absolute permittivity of the piezoelectric crystals and permittivity of free space, respectively. Table 1 listed electrical properties of (*YXt*) −30° cut YCOB crystals with thickness shear vibrations, and compared to non-rotated *YX* cut samples [46]. The properties including the dielectric constant, electromechanical coupling factor, piezoelectric strain coefficient, piezoelectric voltage coefficient, and elastic constant were measured at room temperature, while the electrical resistivity was measured at 950 °C. The dielectric constant was found to be 12.3, maintained the same values for various crystal cuts, while the electromechanical coupling factor k_{26} was found to be 0.19 for *YXt* 0° cut sample, increased to 0.22 for *YXt* −30° cut. Correspondingly, the piezoelectric strain coefficient d_{26} and piezoelectric voltage coefficient g_{26} were around 8 pC/N and 0.07 Vm/N for *YXt* 0° cut samples, increased to 10 pC/N and 0.09 Vm/N for *YXt* −30° cut sample, respectively. Of particular interest is the high mechanical quality factor, being on the order of 9000–16,000 for the thickness shear vibration, together with the high electrical resistivity, being of 2×10^7 Ω cm at elevated temperature of 950 °C, exhibiting the YCOB thickness shear vibration promising for high temperature sensing applications [26,48].

2.3. Sensor assembly

Fig. 4(a) illustrates a schematic cross section of the prototyped shear-mode accelerometer. The overall dimensions of the accelerometer are 30 mm × 26 mm × 17 mm. Four pieces of YCOB crystals (1) were assembled symmetrically on both sides of the center post (2) and rigidly secured via the seismic masses (3) by a bolt (4), washer (5) and nut (6) without using an adhesive connection. The seismic masses and the center post, made of Inconel 601 and electrically isolated from each other, acted as electrical connections. Inconel 601 was used due to its exceptional resistance to high temperature oxidation and corrosion as well as its excellent electrical conductivity [41–43]. The induced charge from each crystal was directly collected through the Inconel center post and seismic masses. The conductivity of Inconel is not as high as that of thin films such as gold and platinum, but the elimination of these films greatly reduces thin film degradation at high temperatures [40]. In this case, the contact condition of surfaces and the applied contact forces between the crystals and Inconel are important factors in sensor performance. A torque control driver (Model 285-50, Wiha Quality Tools) was used to apply a clamping torque to the bolt. One Inconel wire was welded to the side of the base and another wire was clamped between the nut and the seismic mass by the bolt. The bottom of the center post was bonded to an alumina rod (7) using a high temperature adhesive (Resbond 989, Cotronics Corp.). Moreover, for the stable performance of the sensor at high temperatures, temperature limits and thermal expansion effects of each material were considered in the assembly design. Table 2 shows temperature limits and thermal expansion coefficients of materials used in the sensor assembly. Allowable temperatures of all materials are well above the tested temperature range (25–1000 °C). The thermal expansion coefficient of YCOB crystals, α_c (K^{-1}), was estimated by the following equation [49]:

$$\alpha_c(T) = 1.13 \times 10^{-8} \times T + 9.18 \times 10^{-6} \quad (19)$$

The thermal expansion coefficient of Inconel 601, α_I (°C^{-1}), can be estimated by the data sheet from a commercial company (Special Metals, Corp.) as following:

$$\alpha_I(T) = 4.33 \times 10^{-8} \times T + 13.75 \times 10^{-6} \quad (20)$$

Thermal expansion (ΔL) of sensor components along the axis of the bolt and the applied axial force (F) in the bolt were calculated using following equations in order to verify the contact of each component, which is a critical factor for the high temperature sensor operation:

$$\Delta L = \alpha \times \Delta T \times L \quad (21)$$

$$T_B = k_n \times d \times F \quad (22)$$

$$\delta = \frac{FL}{AE} \quad (23)$$

where L is the length of all sensor components along the axis of bolt, T_B is applied torque to the bolt, k_n is a nut factor and d is diameter of the bolt, δ is deformation of the bolt by the applied force and E is Young's modulus.

Fig. 4(b) shows the prototyped shear-mode accelerometer. Sensor components, including crystals, center post, seismic masses and the bolt, underwent thermal expansion when the sensor was exposed to the high temperature environment. This expansion can make a micro connection gap between connected parts due to thermal expansion coefficient differences among materials used. This micro-gap was calculated to be 4.1 μm at 1000 °C, using Eqs. (19)–(21). A clamping torque of 0.6 N m was applied to the bolt for tight contact between crystal and mass, and between crystal and base. This torque compressed seismic masses and crystals by 5 μm which was calculated from Eqs. (22) and (23). As a consequence, the

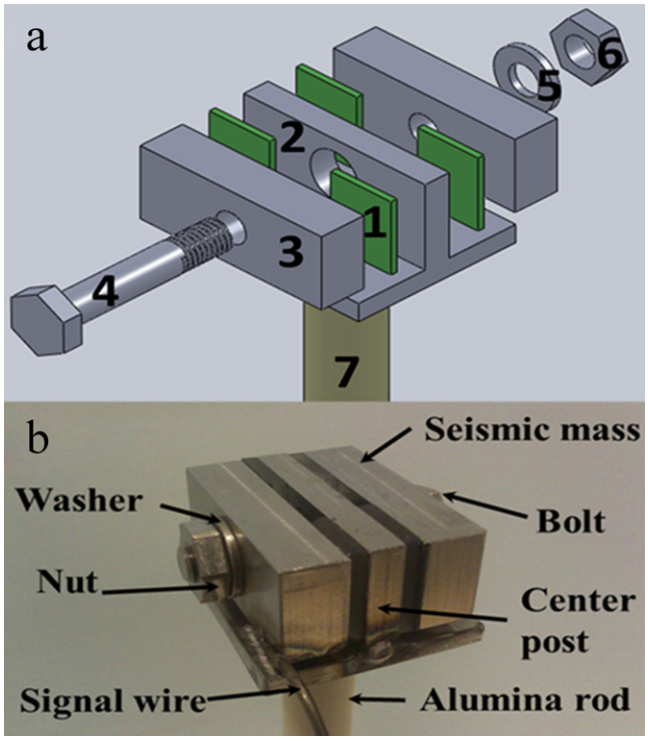

Fig. 4. (a) The expanded view of the sensor assembly and (b) assembled prototyped shear-mode accelerometer.

Table 2
Temperature limits and thermal expansion coefficients of the sensor components.

Material	Temperature limit	Thermal expansion coefficient (ppm/°C)	Young's modulus (GPa)
$YCa_4O(BO_3)_3$	1500 °C (melting temp.)	11.2 @ 1000 °C	55.6 (Shear modulus)
Inconel 601	1411 °C (melting temp.)	17.8 @ 1000 °C	124.7
Adhesive	1648 °C (maximum temp.)	4.5 @ 25 °C	N/A
Alumina	2072 °C (melting temp.)	8.2 @ 25–1000 °C	370.0

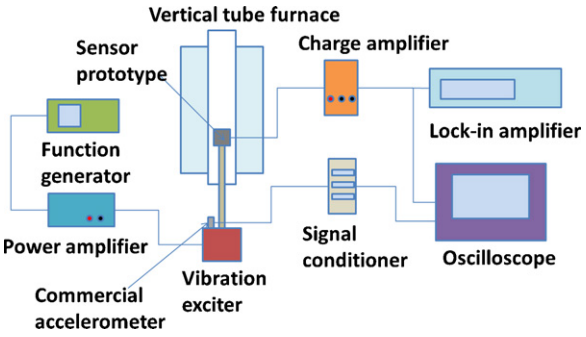

Fig. 5. Experimental setup of high temperature sensor tests.

thermal expansion of sensor components can be ignored, maintaining physical and electrical contact at 1000 °C.

2.4. Experimental setup

The experimental setup for high temperature sensor tests is shown in Fig. 5. The sensor was placed in a vertical tube furnace (Model GSL 1100X, MTI Corporation) through an alumina rod. The alumina rod was bonded to an aluminum bolt and connected to a vibration exciter which can provide a maximum force of 178 N (VG 100, Vibration Test Systems, Inc.). A function generator (Model AFG3101, Tectronix) was used to generate a sinusoidal signal and this signal was amplified by a power amplifier (Type 2706, Bruel & Kjaer), and then applied to the vibration exciter to generate the desired vibration. The output charge signal from the sensing crystals was converted and amplified to voltage signal through a charge amplifier (Type 2635, Bruel & Kjaer), which was recorded through a lock-in amplifier (Model SR830, Stanford Research Systems). The voltage signal was also recorded using an oscilloscope (Model DSO7104B, Agilent Technologies) for transient signal analysis. A commercial accelerometer (Model 352C22, PCB Piezotronics) was used as a reference to measure the acceleration from the vibration exciter. This acceleration was also recorded on the oscilloscope through a signal conditioner (Model 482A16, PCB Piezotronics). In order to reduce the electromagnetic noise, the shaker was shielded by an aluminum foil. The generated charge from the shear-mode accelerometer was recorded as a function of temperature (25–1000 °C), vibration frequency (50–350 Hz), acceleration (0.5–5 g) and high temperature dwell time at 1000 °C.

3. Results and discussion

3.1. Modeling results

Fig. 6 shows an ideal frequency response of the shear-mode accelerometer and a frequency response of the whole sensor system using the model described above. For lower limiting frequency, high resistance of crystals was required because the length of time that the charge can be maintained is proportional to the RC time constant (τ). In this experiment, the crystal resistance (R_{leak} in Eq. (8)) was large enough, and thus, total R was determined dominantly by R_{amp}. As a result, the low-frequency response was determined by the time constant τ of the charge amplifier

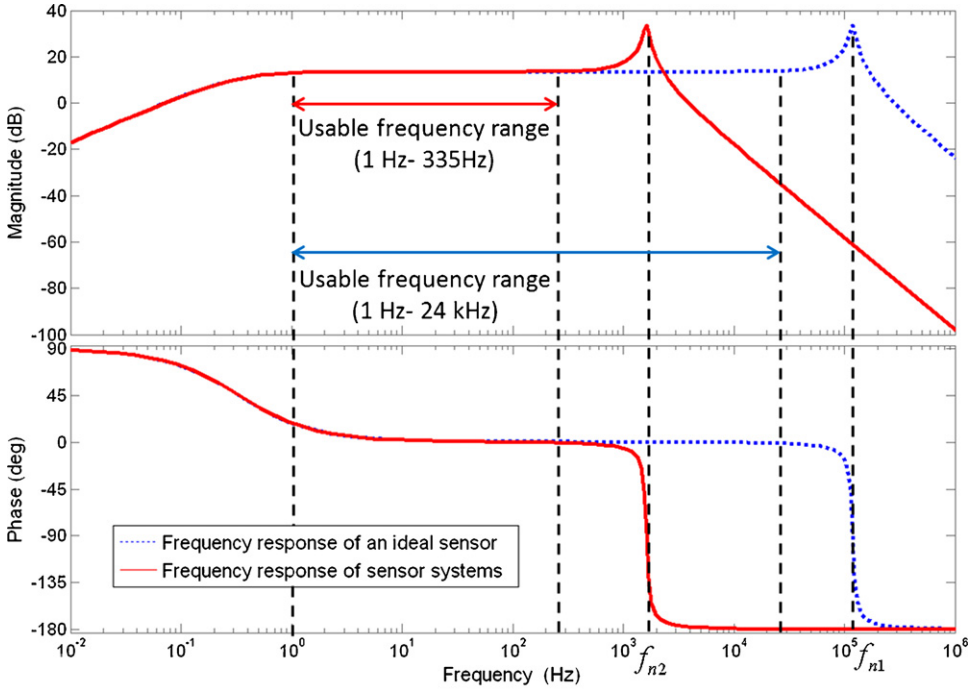

Fig. 6. Frequency response of an ideal sensor (blue line) and frequency response of the sensor system with the rod, mounting bolt and the shaker (red line). (For interpretation of the references to color in this figure legend, the reader is referred to the web version of this article.)

Table 3
Parameters of sensor system model.

Seismic mass (m_1) (kg)	47.68×10^{-3}
Mass of sensor system (m_2) (kg)	407.53×10^{-3}
Spring constant of four crystals (k_1) (N/m)	2.67×10^{10}
Spring constant of sensor system (k_2) (N/m)	4.26×10^{7}
Charge output of unit displacement (k_q) (C/m)	0.27
Capacitance (C) (nF)	1

(1 Hz). The high-frequency response was limited by mechanical resonance of the sensor and other components such as the alumina rod, mounting bolt and the vibration exciter. From Table 3, the modeled accelerometer resonance frequency was calculated to be 120 kHz (f_{n1}) by using Eq. (5). In this case, only the seismic mass of the sensor (m_1) and spring constant of crystals (k_1) were used for the resonance frequency. However, effective spring constant (k_2) and effective mass of the sensor device (m_2) were changed due to the rod, mounting bolt and armature dynamic weight of the shaker. The spring constant of the rod and mounting bolt is lower as compared to those of the other components, so it has a major contribution to the effective spring constant of the sensor system. The effective mass includes the armature mass of the shaker. Thus, the resonance frequency of the sensor system was determined to be 1.6 kHz (f_{n2}). Finite element analysis (FEA) was performed to verify the resonance of the structure. As can be seen Fig. 7, the shear stress of the crystal surfaces, which was directly proportional to the generated charge, showed the highest value at the resonant frequency. From the FEA model, the resonant frequency was found to be 1.9 kHz, which was slightly higher than that of the analytical model. Charge sensitivity (S_Q) of the accelerometer at flat frequency response was calculated to be 4.7 pC/g (=0.48 pC s^2/m) from Eq. (14) using parameters listed in Table 3 (k_q, m_1, k_1, C). As can be seen from Eqs. (7) and (14), the sensitivity of accelerometers is determined by the seismic masses and the piezoelectric constant. Proper sensitivity can be applied to a specific application.

3.2. Experimental results

Fig. 8 shows the tested frequency response of the shear-mode accelerometer at room temperature and at frequencies ranging from 1 Hz to 3 kHz. The resonance frequency and functional frequency range were found to be 1.75 kHz and 1–350 Hz, respectively. The room temperature sensitivity was 5.6 ± 0.11 pC/g, which is higher than modeled sensitivity (4.7 pC/g). This might be caused by the electromagnetic interference (EMI), due to the induced electric field by magnetic field change in the electromagnetic shaker, which affects the output charge of the accelerometer. Fig. 9 illustrates the driving voltage signal from the function generator and the output voltage signal from the charge amplifier as a function of time. There was a 180° phase shift due to the inverting action of the integrator circuit in the charge amplifier. Fig. 10 shows the charge output of the sensor at 1000 °C in different frequency ranges. The sensitivity of the sensor at 1000 °C was found to be 6.3 ± 0.10 pC/g, higher than the room temperature value ~5.6 pC/g, due to temperature dependence of piezoelectric constant of YCOB crystals, being on the order of 10 pC/N and 12 pC/N at room temperature and 1000 °C, respectively [48]. Fig. 11 shows the sensitivity of the prototyped sensor with increasing temperature (25–1000 °C) at the tested frequency range (50–350 Hz). The sensor sensitivity was found to be reasonably stable in the tested temperature range. The average sensitivity was determined to be 5.9 ± 0.06 pC/g throughout the tested frequency and temperature ranges. Fig. 12 shows the sensitivity of the prototyped accelerometer measured for 9 h at 1000 °C. The average sensitivity of the sensor was found to be 6.0 ± 0.12 pC/g during the 9-h dwelling time. Compared to the previous study [44], important parameters, such as the sensor sensitivity and the functional frequency range, showed slightly different values. This is due to the fact that the lock-in amplifier was used here, in order to filter 60 Hz

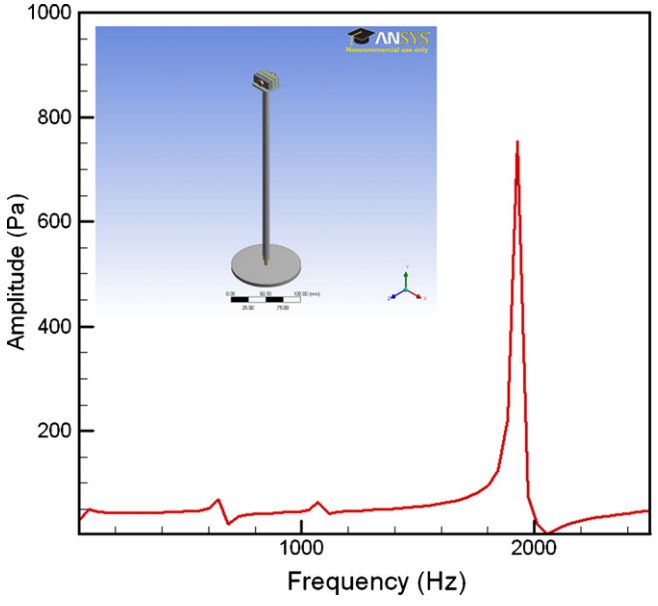

Fig. 7. Finite element analysis of the sensor system using ANSYS. *X*-axis indicates the frequency range and *Y*-axis indicates the shear stress on the surface of YCOB crystal.

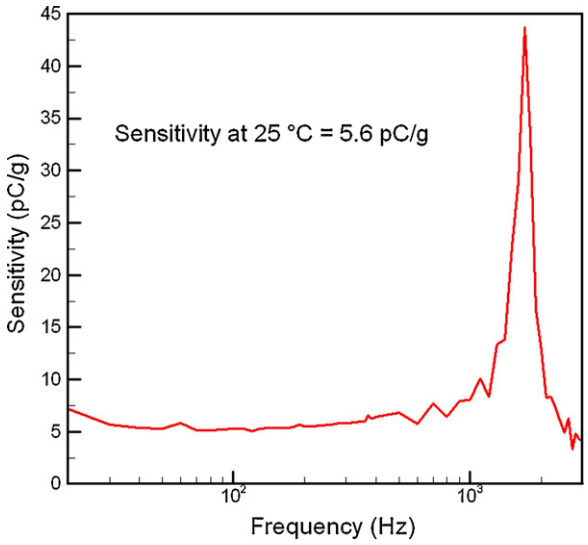

Fig. 8. The tested frequency response of the shear-mode accelerometer at room temperature and at frequencies ranging from 1 Hz to 3 kHz.

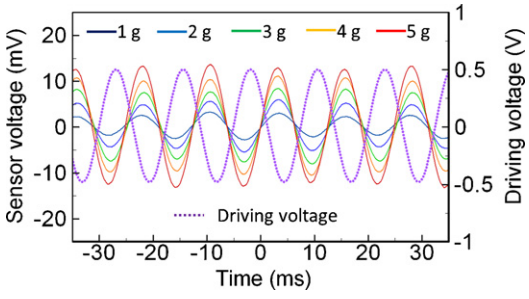

Fig. 9. The driving voltage from the function generator and the output voltage from the charge amplifier.

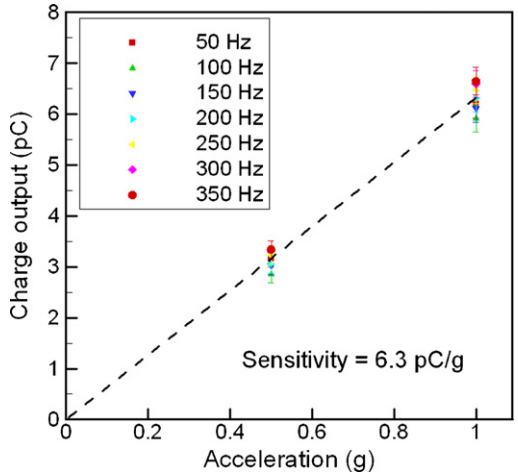

Fig. 10. Sensor charge output as a function of acceleration at 1000 °C.

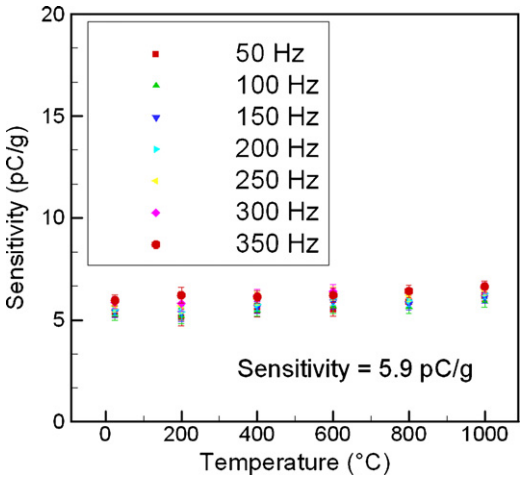

Fig. 11. The sensitivity of the prototyped sensor with increasing temperature (25–1000 °C) at the tested frequency range (50–350 Hz).

power line interference, which can affect the sensor sensitivity. Furthermore, according to the modeling result, the tested frequency range was also changed to a lower frequency to avoid resonance frequency. Table 4 compares the prototyped HT accelerometer to the commercial HT accelerometer. Both accelerometers use the same sensing geometry and output type. The lower resonant frequency of the prototyped sensor can be overcome by reducing the sensor size and weight. Using a thinner YCOB crystal layer will offer higher sensor capacitance and improve the sensor performance. After 9 h, the small crack which generated the noise was found in the ceramic bonding between the base and the alumina rod. The authors believe that this is one of the main reasons of unstable sensor performance after the 9-h dwelling time. Another reason could be the oxidation of the Inconel parts, which can cause reduced electrical conductivity between Inconel and YCOBs. For future work, an Inconel rod will be used instead of the alumina rod and welded to the base to prevent the weak bonding problem. Furthermore, a protective conductive coating will be applied to surfaces of the sensor for more stable and durable performance at higher temperatures up to 1250 °C. More finite-element analyses will be performed to evaluate the effects of resonance modes and thermal expansions at higher temperatures. Finally, the sensor size will be reduced to a micro-scale for low profile sensor mounting in industrial applications. Because of its small size and weight, our miniaturized device will be more suitable for aerospace applications where there are space and weight restrictions. At higher temperatures, small sensors can have higher dimensional stability due to low thermal expansion [50]. The difficulties in fabrication such as micro-machining of Inconel are one of the main problems to be solved in future work.

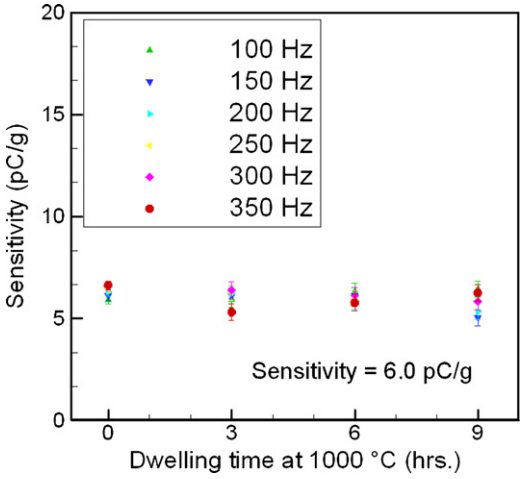

Fig. 12. The sensitivity of the accelerometer as a function of dwell time at 1000 °C.

Table 4
Comparison of prototyped HT accelerometer and commercial HT accelerometer.

	Prototyped HT accelerometer	Commercial HT accelerometer[a]
Sensitivity (pC/g)	5.9	5.0
Frequency range (Hz)	<350	<2500
Resonant frequency (kHz)	1.75	13.5
Temperature limit (°C)	>1000	<649
Capacitance (pF)	50	990
Sensing geometry	Shear	Shear
Output type	Charge	Charge
Housing material	Inconel	Inconel
Size (mm^3)	$30.0 \times 26.0 \times 17.0$	$32.0 \times 16.7 \times 16.7$
Weight (g)	164.0	50.0

[a] Model 357C91, PCB Piezotronics.

4. Conclusions

In conclusion, a shear-mode piezoelectric accelerometer using YCOB single crystals was designed, fabricated, and tested for high temperature vibration sensing applications. Modeling of the accelerometer, YCOB single crystal sample preparation, sensor assembly and experimental setup have been described. From modeling results, the resonance frequency of the sensor system was determined to be 1.6 kHz and the charge sensitivity of the accelerometer at flat frequency response was calculated to be 4.7 pC/g. The sensor tests were conducted in the frequency ranging from 50 Hz to 350 Hz and the temperature ranging from 25 °C to 1000 °C. The sensitivity of the accelerometer was found to be 5.9 ± 0.06 pC/g throughout the tested frequency and temperature range. Furthermore, same sensitivity was observed from the 9-h dwelling test at 1000 °C, revealing high stability and reliability of the accelerometer prototype. Considering modeling, prototyping and testing results, the modeled sensor output agreed reasonably well with the measured results. Higher temperature (~1250 °C) and longer dwelling time test (~100 h) and micro-scale YCOB sensor fabrication will be further explored.

Acknowledgements

This project is sponsored by a NC Space Grant under contract #2010-1662-NCSG Jiang. One of the authors (S. Zhang) would like to thank the support by NSF under contract #ECCS09-25586. The authors would like to thank Dr. Fuh-Gwo Yuan for equipment support.

References

[1] W.J. Fleming, Overview of automotive sensors, IEEE Sensors, Journal 1 (2001) 296–308.
[2] G. Hunter, R. Okojie, P. Neudeck, G. Beheim, G. Ponchak, G. Fralick, J. Wrbanek, L. Chen, High temperature electronics, communications, and supporting technologies for Venus missions, in: Electrical and Electronic Engineering, 2006, pp. 27–30.
[3] S. Zhang, Y. Fei, B.H.T. Chai, E. Frantz, D.W. Snyder, X.N. Jiang, T. Shrout, Characterization of piezoelectric single crystal $YCa_4O(BO_3)_3$ for high temperature applications, Applied Physics Letters 92 (2008) 202905.
[4] S. Zhang, Y. Zheng, H. Kong, J. Xin, E. Frantz, T.R. Shrout, Characterization of high temperature piezoelectric crystals with an ordered langasite structure, Journal of Applied Physics 105 (2009) 114107.
[5] S. Zhang, Y. Fei, E. Frantz, D. Snyder, B. Chai, T. Shrout, High temperature piezoelectric single crystal $ReCa_4O(BO_3)_3$ for sensors, IEEE Transactions on Ultrasonics, Ferroelectrics and Frequency Control 55 (2008) 2703–2708.
[6] O. Boubai, Knock detection in automobile engines, IEEE Instrumentation & Measurement Magazine 3 (2000) 24–28.
[7] A. Carlucci, F. Chiara, D. Laforgia, Analysis of the relation between injection parameter variation and block vibration of an internal combustion diesel engine, Journal of Sound and Vibration 295 (2006) 141–164.
[8] S. Szwaja, K. Bhandary, J. Naber, Comparisons of hydrogen and gasoline combustion knock in a spark ignition engine, International Journal of Hydrogen Energy 32 (2007) 5076–5087.
[9] A.-Q. Mohamad, Exhaust gas temperature for knock detection and control in spark ignition engine, Energy Conversion and Management 37 (1996) 1383–1392.
[10] S. Zhang, X. Jiang, M. Lapsley, P. Moses, T.R. Shrout, Piezoelectric accelerometers for ultrahigh temperature application, Applied Physics Letters 96 (2010) 013506.
[11] G.W. Hunter, J.D. Wrbanek, R.S. Okojie, P.G. Neudeck, G.C. Fralick, L. Chen, J. Xu, G.M. Beheim, Development and application of high-temperature sensors and electronics for propulsion applications, in: Proc. SPIE, 2006, p. 622209.
[12] N.A. Riza, M. Sheikh, F. Perez, Hybrid wireless-wired optical sensor for extreme temperature measurement in next generation energy efficient gas turbines, Journal of Engineering for Gas Turbines and Power 132 (2010) 051601.
[13] X. Jian, M. Bin, Experimental investigation of coupling fiber-optic sensor for vibration measurement, in: IEEE, 2010, pp. 936–939.
[14] U. Dauderstadt, P. De Vries, R. Hiratsuka, P. Sarro, Silicon accelerometer based on thermopiles, Sensors and Actuators A: Physical 46 (1995) 201–204.
[15] H. Seidel, U. Fritsch, R. Gottinger, J. Schalk, J. Walter, K. Ambaum, A piezoresistive silicon accelerometer with monolithically integrated CMOS-circuitry, in: IEEE, 1995, pp. 597–600.
[16] N. Yazdi, F. Ayazi, K. Najafi, Micromachined inertial sensors, Proceedings of the IEEE 86 (1998) 1640–1659.
[17] L. Zimmermann, J.P. Ebersohl, F. Le Hung, J. Berry, F. Baillieu, P. Rey, B. Diem, S. Renard, P. Caillat, Airbag application: a microsystem including a silicon capacitive accelerometer, CMOS switched capacitor electronics and true self-test capability, Sensors and Actuators A: Physical 46 (1995) 190–195.
[18] Z. Lian, Y. JinSong, L. Hao, Conditioning circuit for precise SiC capacitive pressure sensors, in: IEEE, 2011, pp. 559–563.
[19] J.W. Borinski, C.D. Boyd, J.A. Dietz, J.C. Duke, M. Home, Fiber optic sensors for predictive health monitoring, in: IEEE, 2001, pp. 250–262.
[20] R. Turner, P. Fuierer, R. Newnham, T. Shrout, Materials for high temperature acoustic and vibration sensors: a review, Applied Acoustics 41 (1994) 299–324.
[21] M. Schulz, J. Sauerwald, D. Richter, H. Fritze, Electromechanical properties and defect chemistry of high-temperature piezoelectric materials, Ionics 15 (2009) 157–161.
[22] J. Hornsteiner, E. Born, G. Fischerauer, E. Riha, Surface acoustic wave sensors for high-temperature applications, in: IEEE, 1998, pp. 615–620.
[23] R. Fachberger, G. Bruckner, G. Knoll, R. Hauser, J. Biniasch, L. Reindl, Applicability of $LiNbO_3$, langasite and $GaPO_4$ in high temperature SAW sensors operating at radio frequencies, IEEE Transactions on Ultrasonics, Ferroelectrics and Frequency Control 51 (2004) 1427–1431.
[24] G. Ohlendorf, D. Richter, J. Sauerwald, H. Fritze, High-temperature electrical conductivity and electro-mechanical properties of stoichiometric lithium niobate, Diffusion Fundamentals 8 (2008) 6.1–6.7.
[25] D. Damjanovic, Materials for high temperature piezoelectric transducers, Current Opinion in Solid State and Materials Science 3 (1998) 469–473.
[26] S. Zhang, F. Yu, Piezoelectric materials for high temperature sensors, Journal of the American Ceramic Society 94 (2011) 3153–3170.
[27] H. Fritze, H. Seh, H. Tuller, G. Borchardt, Operation limits of langasite high temperature nanobalances, Journal of the European Ceramic Society 21 (2001) 1473–1477.
[28] H. Fritze, H. Tuller, Langasite for high-temperature bulk acoustic wave applications, Applied Physics Letters 78 (2001) 976–977.
[29] H. Fritze, High-temperature bulk acoustic wave sensors, Measurement Science and Technology 22 (2011) 012002.
[30] C.M. Lin, T.T. Yen, V.V. Felmetsger, M.A. Hopcroft, J.H. Kuypers, A.P. Pisano, Thermally compensated aluminum nitride Lamb wave resonators for high temperature applications, Applied Physics Letters 97 (2010) 083501.
[31] T.T. Yen, C.M. Lin, X. Zhao, V.V. Felmetsger, D.G. Senesky, M.A. Hopcroft, A.P. Pisano, Characterization of aluminum nitride Lamb wave resonators operating at 600 °C for harsh environment RF applications, in: Proceedings of the IEEE International Conference on Micro Electro Mechanical Systems, IEEE, MEMS, Hong Kong, 2010, pp. 731–734.
[32] R. Kažys, A. Voleišis, B. Voleišien, High temperature ultrasonic transducers: review, Ultragarsas (Ultrasound) 63 (2008) 7–17.
[33] M.P. da Cunha, T. Moonlight, R. Lad, D. Frankel, G. Bernhard, High temperature sensing technology for applications up to 1000 °C, in: IEEE, 2008, pp. 752–755.
[34] J. Puigcorbé, D. Vogel, B. Michel, A. Vilà, I. Gràcia, C. Cané, J. Morante, High temperature degradation of Pt/Ti electrodes in micro-hotplate gas sensors, Journal of Micromechanics and Microengineering 13 (2003) S119.
[35] K.W. Kim, E.H. Lee, J.S. Kim, K.H. Shin, B.I. Jung, A study on performance improvement of Ir oxide-coated titanium electrode for organic destruction, Electrochimica Acta 47 (2002) 2525–2531.
[36] R. Vedula, C. Desu, S. Tirumala, H. Bhatt, S. Desu, K. Lee, New electrode-barrier structures for high density ferroelectric memories, Applied Physics A: Materials Science & Processing 72 (2001) 13–20.
[37] J. Thiele, M.P. da Cunha, High temperature LGS SAW gas sensor, Sensors and Actuators B: Chemical 113 (2006) 816–822.
[38] J.A. Thiele, M.P. da Cunha, Platinum and palladium high-temperature transducers on langasite, IEEE Transactions on Ultrasonics, Ferroelectrics and Frequency Control 52 (2005) 545–549.
[39] J.G. Lisoni, J.A. Johnson, J.L. Everaert, L. Goux, H.V. Meeren, V. Paraschiv, M. Willegems, D. Maes, L. Haspeslagh, D.J. Wouters, C. Caputa, R. Zambrano, Mechanical stability of Ir electrodes used for stacked $SrBi_2Ta_2O_9$ ferroelectric capacitors, Integrated Ferroelectrics 81 (2006) 37–45.
[40] D. Frankel, G. Bernhardt, B. Sturtevant, T. Moonlight, M. Pereira da Cunha, R. Lad, Stable electrodes and ultrathin passivation coatings for high temperature sensors in harsh environments, in: IEEE, 2008, pp. 82–85.
[41] L. Starck, Accelerometer, U.S. Patent (1996).
[42] J.M. Kubler, M.D. Insalaco, Shear accelerometer, U.S. Patent (1996).
[43] K. Kishi, Y. Ooishi, H. Noma, E. Ushijima, N. Ueno, M. Akiyama, T. Tabaru, Measurement of output voltage of aluminum nitride thin film as a pressure sensor at high temperature, Journal of the European Ceramic Society 26 (2006) 3425–3430.
[44] K. Kim, S. Zhang, W. Huang, F. Yu, X. Jiang, $YCa_4O(BO_3)_3$ (YCOB) high temperature vibration sensor, Journal of Applied Physics 109 (2011) 126103.
[45] J.C. Yu, C.B. Lan, System modeling of microaccelerometer using piezoelectric thin films, Sensors and Actuators A: Physical 88 (2001) 178–186.
[46] S. Zhang, F. Yu, R. Xia, Y. Fei, E. Frantz, X. Zhao, D. Yuan, B.H.T. Chai, D. Snyder, T.R. Shrout, High temperature ReCOB piezocrystals: recent developments, Journal of Crystal Growth 318 (2011) 884–889.
[47] A. Meitzler, IEEE Standard on Piezoelectricity, Society, ANSI/IEEE Standard 176-1987, 1988.
[48] F. Yu, S. Zhang, X. Zhao, D. Yuan, Q. Wang, T.R. Shrout, High temperature piezoelectric properties of yttrium calcium oxyborate single crystals, Physica Status Solidi (RRL) – Rapid Research Letters 4 (2010) 103–105.
[49] P. Segonds, B. Boulanger, B. Ménaert, J. Zaccaro, J. Salvestrini, M. Fontana, R. Moncorgé, F. Porée, G. Gadret, J. Mangin, Optical characterizations of $YCa_4O(BO_3)_3$ and $Nd:YCa_4O(BO_3)_3$ crystals, Optical Materials 29 (2007) 975–982.
[50] T.R. Hsu, MEMS and Microsystems: Design, Manufacture, and Nanoscale Engineering, Wiley, 2008.

Biographies

Kyungrim Kim received his B.S. in Mechanical and Automotive Engineering from Kookmin University in Korea. In Fall 2009, he started his work as a Ph.D. student in the Department of Mechanical & Aerospace Engineering, North Carolina State University. Currently, he is working as a Research Assistant at the Micro/Nano Engineer Laboratory under Dr. Jiang. His main research interest is high temperature piezoelectric sensors.

Shujun Zhang received Ph.D. degree from The State Key Lab. of Crystal Materials, Shandong University, China, in 2000. He is currently a Senior Research Associate at Material Research Institute and Associate Professor at Materials Science and Engineering Department of The Pennsylvania State University. He is an associate editor for Journal of the American Ceramic Society. He is a senior member of IEEE-UFFC chapter and member of American Ceramic Society. He holds one patent and has coauthored more than 180 papers in the area of functional single crystals and ceramics.

Giovanni Salazar received his B.S. in Mechanical and Aerospace Engineering from North Carolina State University in 2011. Now he is a graduate student working as a Research Assistant at the Micro/Nano Engineer Laboratory under Dr. Jiang. His current research field is sensors for extreme environment.

Xiaoning Jiang received his Ph.D. from Tsinghua University in 1997 and Postdoctoral trainings from Nanyang Technological University and the Pennsylvania State University (1997–2001). He worked in industry (Standard MEMS, Inc. and TRS Technologies, Inc.) before joining North Carolina State University in 2009 as an Associate Professor of Mechanical and Aerospace Engineering. Dr. Jiang is the author and co-author of two book chapters, one book, more than 12 US patents and patent applications and over 50 technical papers and presentations on piezoelectric composite micromachined ultrasound transducers (PC-MUT), ultrasound for medical imaging and NDE, smart materials and structures and M/NEMS.